Lab on a Chip

View Online / Journal Homepage / Table of Contents for this issue
Dynamic Article Links

Cite this: *Lab Chip*, 2012, **12**, 2970–2976

www.rsc.org/loc

METHOD

UV epoxy bonding for enhanced SAW transmission and microscale acoustofluidic integration†

Sean M. Langelier,[b] Leslie Y. Yeo[a] and James Friend*[ab]

Received 23rd January 2012, Accepted 3rd May 2012
DOI: 10.1039/c2lc40085e

Downloaded by Monash University on 19 July 2012
Published on 10 May 2012 on http://pubs.rsc.org | doi:10.1039/C2LC40085E

Surface acoustic waves (SAWs) are appealing as a means to manipulate fluids within lab-on-a-chip systems. However, current acoustofluidic devices almost universally rely on elastomeric materials, especially PDMS, that are inherently ill-suited for conveyance of elastic energy due to their strong attenuation properties. Here, we explore the use of a low-viscosity UV epoxy resin for room temperature bonding of lithium niobate ($LiNbO_3$), the most widely used anisotropic piezoelectric substrate used in the generation of SAWs, to standard micromachined superstrates such as Pyrex® and silicon. The bonding methodology is straightforward and allows for reliable production of sub-micron bonds that are capable of enduring the high surface strains and accelerations needed for conveyance of SAWs. Devices prepared with this approach display as much as two orders of magnitude, or 20 dB, improvement in SAW transmission compared to those fabricated using the standard PDMS elastomer. This enhancement enables a broad range of applications in acoustofluidics that are consistent with the low power requirements of portable battery-driven circuits and the development of genuinely portable lab-on-a-chip devices. The method is exemplified in the fabrication of a closed-loop bidirectional SAW pumping concept with applications in micro-scale flow control, and represents the first demonstration of closed channel SAW pumping in a bonded glass/$LiNbO_3$ device.

Chip-based fluidic actuators using surface acoustic waves (SAWs) have become popular among microfluidic practitioners, who continue to explore new applications in acoustofluidic integration.[1–3] Despite only being recently demonstrated, the pairing of SAW and standard microfluidic structures has already proven useful for structure-independent mixing enhancement,[4,5] generation of macromolecule seeded aerosols and nanoparticles for pulmonary drug delivery,[6,7] particle separation and concentration,[8–12] surface micro-patterning,[13] *ELISA* automation and binding enhancement,[14,15] and development of rotational micromotors for MEMS.[16]

Still, the most tantalizing prospects in acoustofluidics lie in fluidic actuation. Of particular interest is the development of self-contained micropumps for precise fluid metering within branched microchannel networks. Versatile and reliable pumping of this type is perhaps possible acoustically, owing to the enormous surface accelerations, weak viscous dependence, and low power demands (relative to conventional displacement or pneumatic approaches) of acoustically driven flows. If successful, such pumps would solve perhaps the single most limiting and sustained issue facing so-called Lab-on-a-Chip (LOC) systems: the tethering of a device to bench scale infrastructure. With SAWs, high hopes stem from acoustic theory that suggests a potential sidestepping of the scaling limitations typical of pressure driven flows[2,17,18] by the leveraging of non-linear viscous effects of high amplitude SAWs. However, realization of such predictions has proven challenging owing mainly to difficulties in fabrication. Principally, these difficulties relate to the bonding of piezoelectric materials which, when joined using conventional electrothermal routes, produce tremendous interfacial stresses[19,20]—an issue reflected in the fact that nearly all SAW micropumps that have been developed to date are employ open channels or planar, chemically treated, surfaces.[21–23] Alternative techniques such as surface activated bonding using an argon beam,[24] for example, have somewhat addressed this issue by allowing room temperature processing, but, such methods require sample manipulation within high-vacuum environments and a notably atypical vacuum chamber configuration (for example, the MWB-04 by Sojitsu Manufacturing/Mitsubishi Heavy Industries, Tokyo, Japan), making this route both impractical and prohibitively expensive. As a consequence, researchers have turned to soft lithography,[25] a popular molding technique using a cast liquid elastomer, typically polydimethylsiloxane (PDMS), in order to form microchannels.[3,26,27]

[a]*MicroNanophysics Research Laboratory, School of Electrical and Computer Engineering, RMIT University, Melbourne Australia. E-mail: james.friend@rmit.edu.au; Fax: +61 3 9925 2007; Tel: +61 3 9925 4059*
[b]*Melbourne Centre for Nanofabrication, 151 Wellington Road, Clayton Australia*
† Electronic supplementary information (ESI) available. See DOI: 10.1039/c2lc40085e

 This journal is © The Royal Society of Chemistry 2012

Published on 10 May 2012 on http://pubs.rsc.org | doi:10.1039/C2LC40085E
Downloaded by Monash University on 19 July 2012

Unfortunately, these elastomers strongly attenuate SAWs, giving rise to operational drawbacks such as intense heat generation, suppression of acoustic radiation, and excessive power consumption. These losses, often ignored or glossed over in the literature, severely limit the transmission of acoustic energy into the working fluid.

The goal of acoustofluidic integration—apart from issues of device design and application area—is efficient delivery of acoustic energy into the working fluid. However, because the vast majority of SAW energy resides at the material surface (see amplitude decay with substrate depth in Fig. 1a and 1b), bound structures in the path of a propagating SAW can have a profoundly detrimental effect on transmission leading to severe reflections, undesirable resonance, and attenuation or damping.[28,29]

Toward addressing these issues, we describe an alternative bonding technique, using a low viscosity, low shrinkage, UV-curable epoxy resin (NOA 61, Norland Optical Adhesives, Cranbury, New Jersey USA), that enables robust adhesion of standard machinable substrates such as glass and silicon and SAW grade piezoelectrics at standard temperature and pressure. Use of these rigid materials in conjunction with a stiff epoxy guiding layer enables far superior transmission of acoustic energy (see Fig. 1a and 1b). The selection of this epoxy was made on the basis of the low viscosity and shrinkage characteristics; since there are many UV-curable epoxies with such characteristics more commonly used in glass repair, there are certainly many other choices that would work equally well in this application. The bonding process is as follows: (i) surfaces are cleaned and brought into intimate contact, (ii) an optional compressive load is applied using either an arrangement of point loads or a parallel plate clamp, (iii) the microscopic air gap between the two surfaces is loaded with the epoxy resin *via* capillary pressure-driven flow, and (iv) the bond is formed by cross-linking the epoxy under UV light. Devices prepared using this approach display remarkable enhancement in SAW

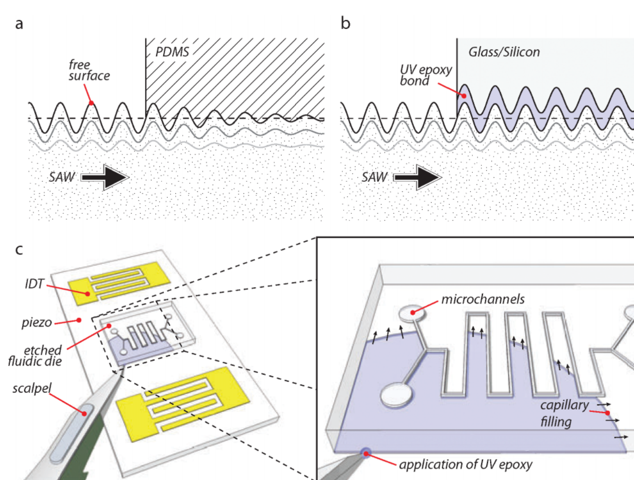

Fig. 1 Summary of bonding concept. (a) Lossy SAW transmission through PDMS elastomer. (b) Relatively unattenuated SAW transmission through rigid UV epoxy. (c) Schematic of UV epoxy bonding application driven by spontaneous capillary filling (*inset*) at room temperature. Compressive loading and UV exposure not shown. Note: typical SAWs are nanometers in amplitude and figures are not drawn to scale.

transmission (up to two orders of magnitude or 20 dB) when compared to those fabricated using soft lithography with PDMS (Sylgard 184, Dow Corning, Auburn, Michigan USA) mixed in a 1 : 10 standard base : catalyst ratio nearly ubiquitous in the fabrication of microfluidics devices.[30] These gains in SAW transmission grant substantial energetic savings by facilitating device portability and minimizing mechanical fatigue. An inherent benefit of this approach is that it is performed at room temperature and atmospheric conditions, thus eliminating the aforementioned issues of interfacial stress and the need for manipulation under high vacuum. Another advantage of this approach is that bond thicknesses become tailorable—*via* adjustment of the clamping force—over the range of $\sim$0.1 to 4 μm granting additional freedom in the design of fluidic structures. Moreover, cured bonds are tolerant to a variety of solvents and are more or less insensitive to choice of bonded materials. In addition to devices built expressly for SAW transmission and bond characterization, we also present the first example of a closed-channel SAW-driven glass $LiNbO_3$ pump prepared using this approach.

Components are first cleaned by placing them in an ultrasonically agitated acetone bath for approximately 1 min, followed by a thorough rinse in isopropanol, and finally, dried in a jet of nitrogen. Bonding surfaces are then carefully brought into contact at which point the formation of broadly spaced ($\geqslant$1 mm) interference fringes—an effect related to the difference in optical path length of the air wedge between the mating surfaces—are used as a qualitative indication of surface cleanliness. Tightly spaced fringes, if observed, indicate either trapped particulates (from improper cleaning) or surface defects. Optionally, after a quality surface mating is obtained, a compression force is applied to the material stack to effect predictable control over the dimension of the capillary air gap and, by extension, the final bond thickness upon curing of the adhesive. In the experiment to be described, modest compression forces were administered by applying symmetric point loading on the surface of superstrate using spring loaded pogo probes (0906-1, Mill-Max, Oyster Bay, New York) mounted within custom 3D-printed jigs (see supplemental information†). Individually, these probes supply $\approx$ 10–12 kPa of force. Larger compression forces ($\approx$2000 kPa) were also administered using a spring-loaded parallel-plate clamp.

Alignment of microfluidic structures with SAW components, when needed, was greatly facilitated by the application of a loading force. For alignment within the clamping jig, use of rigid spacers such as glass slides were found to sufficiently increase device access, allowing for manual alignment with lithographically defined markers. In each case, the use of a low magnification microscope was indispensable during the alignment step. Following application of the adhesive, to be discussed shortly, bonds were cured by exposure to a 20 W, 254 nm UV light (XX-20S-Mineralight, Krackeler Scientific, Albany, New York) for 7 min followed by an optional post-exposure aging for 12 h at 55 °C. Ageing did not have a significant effect on the transmission of SAW for the frequencies examined here.

Adhesive was introduced by placing a small ($<$1 μL) bead of epoxy at one or more junctions of the piezoelectric and superstrate materials using the tip of a scalpel or a small, fine tipped brush, as shown in Fig. 1c. The low viscosity and surface

Downloaded by Monash University on 19 July 2012
Published on 10 May 2012 on http://pubs.rsc.org | doi:10.1039/C2LC40085E

tension of the liquid epoxy (0.3–0.4 Pa s) enables spontaneous capillary penetration of the adhesive into the narrow air space formed between the two bonding surfaces. Because steep changes in hydraulic resistance near lithographically defined features–which appear as large abrupt expansions to the advancing epoxy–serve to confine the advancing liquid front, delivery is limited to only those areas that are in direct or intimate contact and not in the microchannels themselves, see *inset*, Fig. 1c. However, patience and care during this step is critical, as liberal application of adhesive will increase the likelihood of channel flooding. These risks become markedly more significant in devices with very shallow etch depths and/or lateral channel dimensions $\leqslant$ 5 μm. It is also worth noting that for designs with enclosed regions (*i.e.*, bonding areas that are hydraulically inaccessible), adhesive can be delivered *via* pre-drilled access holes. Alternatively, epoxy may be applied using a stamping approach,[31] but, this approach is inherently prone to channel flooding, bond irregularities, and voids, and as such will not be discussed here.

To examine the effect of external clamping force on the final bond thickness, test devices were subjected to various compressive loads during the gluing process. Cross-sections of bonded devices (prepared with a high speed, diamond impregnated rotary saw fitted with a 200 μm wide blade) were subsequently analyzed using a scanning electron microscope (SEM). In order to probe the effect of user variability on the final bond thickness, specifically to procedural differences in adhesive application–important here as user skill and patience will vary and may significantly effect the result–two means of epoxy application were tested: (1) *Post-load*; in which epoxy was applied liberally and/or carelessly prior to compressive loading, and (2) *Pre-load*; in which compressive loads were applied prior to the introduction of the adhesive which, in this scenario, was done so sparingly, and step-wise until the entire bonded interface was primed with epoxy. Bond curing in the former was performed just moments after the administration of the compressive load in order to probe for unwanted thickness effects related to the hydraulic squeeze out time the glue. Test devices for bond thickness characterization and SAW transmission (to be discussed shortly) were fabricated by bonding a bare borosilicate superstrate (0.5 cm × 1.0 cm) to a piece of SAW-grade 128°Y-cut, X-propagating $LiNbO_3$ (2.5 cm long × 1.6 cm wide × 0.5 mm thick).

Bond thickness results and example SEM cross-sections are presented in Fig. 2. Data were obtained by subjecting devices (sets of) to compressive loads of either 0.01, 20, 40, or 2000 kPa. This loading was accomplished using, respectively, 0, 2, and 4 pogo probes for the smaller loads and a spring-loaded clamping jig for the highest load. An immediate observation we can make from Fig. 2a is the marked difference in bond thickness–most notably at minuscule loadings–between the two means of epoxy application described above. See Fig. 2a (*inset*) for a schematic representation of a sectioned device. Using a minimum loading, for example, where no external pressure is applied to the stack, the measured bond thickness was found to be 4.0 ± 0.4 μm and 1.2 ± 0.5 μm for *post-load* and *pre-load* prepared devices, respectively. This large difference in bond thickness, as we might suspect, reflects the inherent sensitivity of the approach to adhesive application in the absence of a

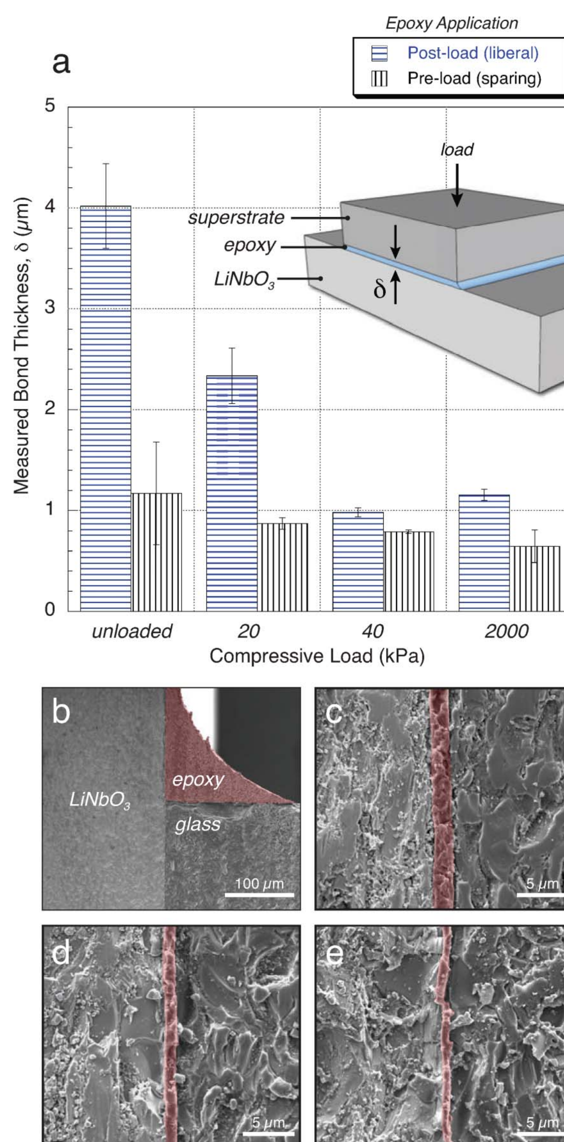

Fig. 2 Bond thickness and compressive loading with adhesive application method. (a) SEM measured bond thickness subject to various compressive loads using both *pre* and *post-load* methods. (a, *inset*) Schematic representation of sectioned device illustrating the transverse bond thickness, *δ*. (b–e) False colored SEM cross-section images of bonded devices highlighting range of thicknesses from (a).

compressive loading. Clearly, the liberal application of the adhesive is serving to float the superstrate dies, thus resulting in a larger bond interface. However, we must note that using the *pre-load* approach, it was possible to obtain bonds with a dimension $\leqslant$ 1 μm. This dimension, as it turns out, is rather significant in the context of the majority of SAW microfluidic systems.

Compressive loading ostensibly does away with the variability between these two approaches by overcoming the liquid surface tension which would otherwise serve to lift the superstrate die. Notice that with sparing application of the adhesive (*pre-load*), as described above, it is trivial to obtain 1.2 ± 0.5 μm bond interfaces even without compressive loading that, in terms of device application, is perfectly adequate for the vast majority of microfluidic applications. However, if sub-micron interfaces are

This journal is © The Royal Society of Chemistry 2012

View Online

Published on 10 May 2012 on http://pubs.rsc.org | doi:10.1039/C2LC40085E
Downloaded by Monash University on 19 July 2012

required, a modest amount of compression ($\geqslant$40 kPa) was found to routinely yield bonds with a thickness $\leqslant$ 780 $\pm$ 20 nm. Application of additional clamping pressure of approximately 2000 kPa appears to give diminishing returns with respect to the measured bond thickness, resulting in bonds with an average dimension of 647 $\pm$ 16 nm. Experiments were also performed using a precision machined mechanical vise for delivery of extremely high compressive loads. Using the vise, bond thicknesses were found to be significantly reduced ($\approx$100–200 nm). These results have been omitted here owing to issues with adequate optical access (necessary for the UV exposure) and load quantification. For the purposes of this work, it is sufficient to note that, if desired, thinner bonds can be produced under very high loading. SEM images of bonded cross sections reveal conformal bonding between the epoxy, glass, and $LiNbO_3$ with no evidence of delamination. For visual reference, several sample false colored SEM images of examined devices are shown in Fig. 2(c–e) for loadings of 0.01, 20 and 40 kPa, respectively. An example image of a bond formed from the mechanical vise is available in the supplemental material†.

Transmission of SAW energy through surface obstructions primarily depends upon the dimensions of the bonded structure, relative to the SAW wavelength, and its material properties, specifically, the modulus of elasticity. Wave attenuation from the former derives from complex wave interference—analogous to oblique refraction in certain optical systems—that becomes more severe as the wavelength of the incident SAW becomes small relative to the transverse dimension of the bonded structure, here defined as the thickness of the bonded interface δ. In the latter case, attenuation originates mainly from gradients in deformation at the SAW/bond interface, an effect that, as one might imagine, is more pronounced for rubbery compliant materials such as PDMS than it is for more rigid or glassy materials. Other factors such as temperature and thermal expansion can also significantly impact SAW transmission, but such effects can often be ignored at temperatures well below the glass transition temperature of the material.

In Fig. 3, SAW transmission for devices of several different operating frequencies are plotted in relation to the measured bond thickness. Test devices consisted of a pair of planar comblike interdigital transducers (IDTs)—the dimensions of which dictate, among other things, the location of the center SAW frequency band—arranged in a delay-line configuration on either side of a bonded superstrate (see *inset*, Fig. 3a). Devices were inserted into a measurement jig connected to a high frequency network analyzer (Agilent E5062A, Santa Clara, CA) and the transmission coefficient, defined as the ratio of the transmitted to incident power as communicated between the source and receiver IDTs, was recorded over a range of input frequencies about the SAW band center. As an example, the average transmission coefficient measurements for the 32.7 MHz set of devices are plotted in Fig. 3a. The data shows a dramatic improvement in SAW transmission with a thinner bond interface, a result which qualitatively is in agreement with diminished refraction/interference-derived attenuation mentioned earlier. In addition, these devices display as much as two orders of magnitude or +20 dB improvement in SAW transmission as compared to identical devices fabricated using bonded PDMS superstrates. Again, the practical upshot of this improved efficiency is a reduction in device operating power and mechanical fatigue (two highly desirable features of portable LOCs) as well as a reduction in heat generation, which will help to preserve the viability of biological analytes. Even the poorest performing devices, *i.e.*, those corresponding to a bond thickness

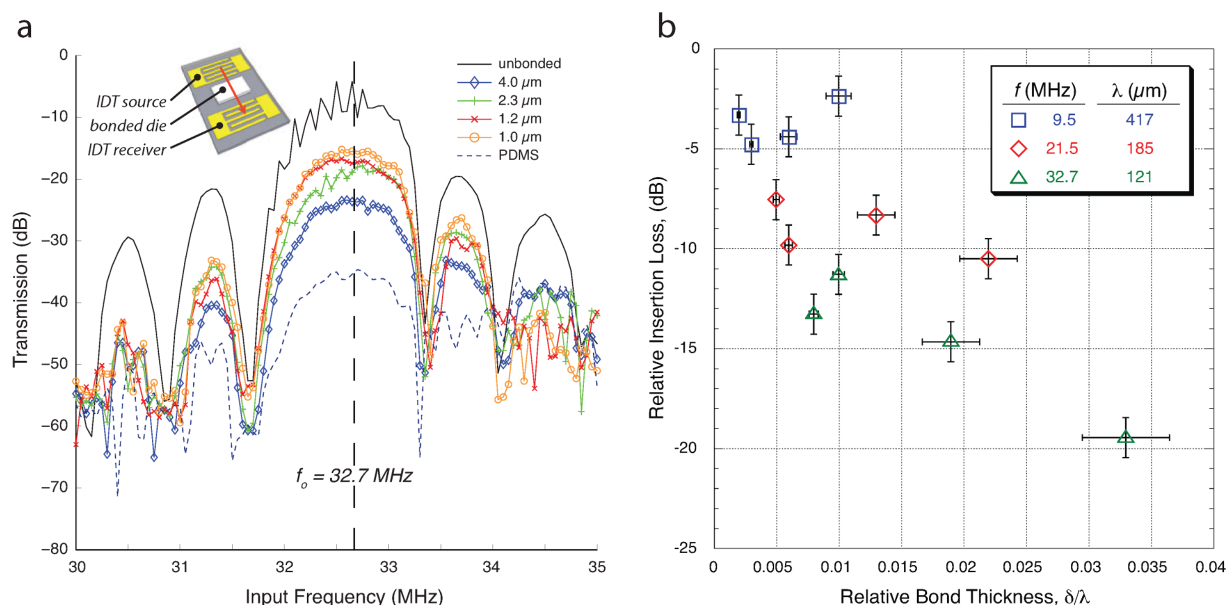

Fig. 3 Effect of bond thickness and frequency on SAW transmission. (a) Network analyzer transmission results for 32.7 MHz devices illustrating the enhancement of SAW transmission with decreasing bond thickness as compared to bonded PDMS devices of the same geometry. (b) Insertion loss relative to transmission in the unbonded case which shows the marked improvement of SAW transmission with decreasing bond thickness as well as the diminishing returns at lower frequencies. Here, the IDT aperture was 7 mm wide, the IDTs were separated by a distance of 12.8 mm along the X axis, and the 0.5 mm-thick glass dies were 5 mm long along the X axis and 10 mm wide, aligned to the centerline of and spanning the full aperture, and placed equidistant from each IDT.

Published on 10 May 2012 on http://pubs.rsc.org | doi:10.1039/C2LC40085E
Downloaded by Monash University on 19 July 2012

of ≈ 4.0 μm, show enhancement of +12 dB. Examining the results carefully, there does appear to be some variation in the relative insertion loss with respect to the relative bond thickness, because the effective coupling of modal excitation within the epoxy layer is strongly dependent upon its thickness. It remains to be seen whether there is an ideal thickness for this layer, perhaps one-quarter of a wavelength, to minimize energy losses.

But these improvements in transmission are not universal and do depend upon SAW frequency. In looking at transmission profiles from devices with different operating frequencies, as shown in Fig. 3b, we note that an increase in SAW frequency from 9.5 to 32.7 MHz is accompanied by a corresponding increase in the relative insertion loss (defined here as the difference in the transmission coefficient at the band center for the bonded and unbonded or open IDT case). This attenuation is predominantly a result of inherent SAW scattering within the piezoelectric substrate and is roughly proportional to the square of the operating frequency.[29] A portion of this attenuation can also be attributed to the number of IDT finger pairs between devices of different frequency, which was not maintained here, opting instead for fixed overall device dimensions. As such, the number of electrode pairs were fixed at 12, 28, and 41 for the 9.5, 21.5 and 32.7 MHz devices, respectively. Readers should note that the use of fewer electrode finger pairs has a negative impact on the quality factor of the SAW resonance by effectively spreading the resonant response of the system over a broader range of frequencies, thus lowering the amplitude of the SAW at the band center. We also note a second damping effect that tracks with the increase in the relative bond thickness. This damping, especially pronounced in the higher frequency devices, is indicative of bonds no longer behaving as acoustically thin ($\delta \ll \lambda$) conduits. In such cases, the gradient in surface displacement at the interface, which can be neglected for an acoustically thin film,[28] gives rise to a phase lag in the film bulk and thus increased attenuation. For the devices and frequencies tested, it was found that a relative bond thickness above 0.015 resulted in markedly increased damping. This damping at higher frequencies places practical limits on the SAW frequencies which may be used with this method. However, substantial decreases in the bond thickness are possible with application of considerable clamping forces. It is also important to note that the vast majority of acoustofluidic demonstrations in the literature utilize devices in the range of 10–50 MHz,[2] well within the capabilities of this approach. In our testing, none of the several tens of devices suffered bond failures over the hundreds of hours of testing we performed in preparing the results for this study. With proper attention to detail, the UV epoxy bond appears to be quite capable of handling the extraordinary accelerations induced by the SAW transmission.

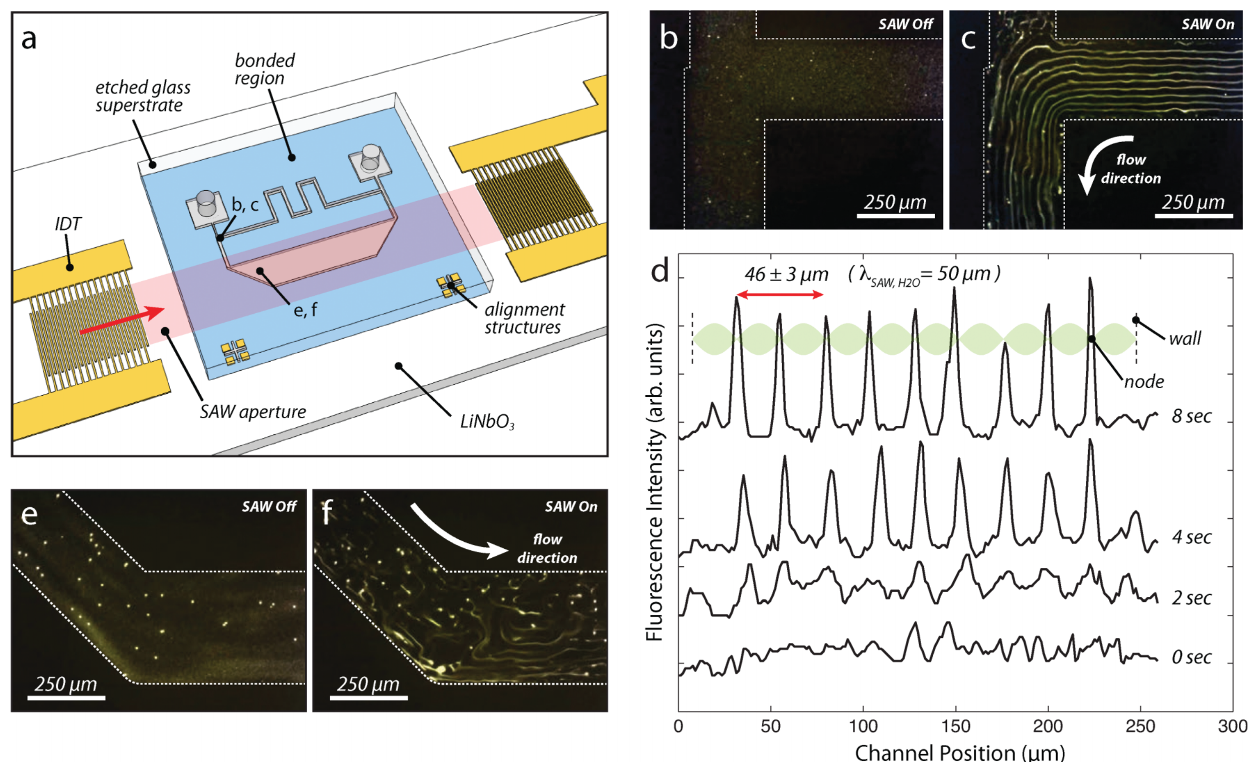

Fig. 4 Closed channel SAW pumping in bonded glass microchannels. (a) Schematic representation of the test device with an arrow highlighting the relevant SAW direction. (b–f) SAW *On* and *Off* dynamics of 0.2 and 5.0 μm fluorescent tracer particles within an approximately 250 μm wide by 29.6 μm deep microchannel. (b-c) Persistent standing wave behavior outside of the SAW aperture with unidirectional anti-clockwise flow. (d) Time sequence of (b-c) transition with schematic representation of relevant nodal spacing. (e-f) Apparently chaotic streaming and particle aggregation in the presence of a net flow in the channel test segment which lies within the SAW aperture at the side nearest to the leftward approaching SAW. Here, the IDT was composed of 25 finger pairs with a designed wavelength of 120 μm and a finger and gap width of, each, 30 μm. The IDT aperture was 2 mm wide, the IDTs were separated by a distance of 10 mm along the X axis, and the etched glass superstrate was 5 mm long × 5 mm wide × 0.5 mm thick and was placed equidistant from each IDT.

 This journal is © The Royal Society of Chemistry 2012

Downloaded by Monash University on 19 July 2012
Published on 10 May 2012 on http://pubs.rsc.org | doi:10.1039/C2LC40085E

For completeness, a demonstration of the presented methodology for applications in acoustic flow generation and control is shown in Fig. 4. Devices consisted of 128°YX $LiNbO_3$ outfitted with a pair of 32 MHz IDTs straddling an etched glass superstrate. Dies were bonded under approximately 40 kPa of load according to the *pre-load* procedure described above and as such should possess an $\approx$ 1 μm bond. The fluidic design featured a pair of inlet and outlet ports, a serpentine segment, and a channel test segment positioned inside the projected SAW aperture. A schematic representation of the test devices is shown in Fig. 4a. Prior to experiment, the flow loop was primed with deionized water seeded with 0.2 and 5.0 μm fluorescent microparticles. Flow was induced by application of a 32 MHz AC signal at a power of approximately 400 mW to a specified IDT. Bulk flow, occurring in the propagation direction of the impinging SAW, was immediately apparent upon application of the RF signal. To the best of our knowledge, this represents the first report of a bonded glass/$LiNbO_3$ microfluidic system driven by SAW. The angled features at either end of the channel test segment were used as microfluidic expansion regions, but they also serve to avoid direct reflection of acoustic radiation back towards the source. Curiously, they act to transmit the acoustic radiation carried in the fluid along another route.

Outside of the projected SAW aperture, persistent acoustic reflections within the fluid and superstrate give rise to standing waves which serve to concentrate particles along the various pressure nodes during flow. This transition from a uniform seeding to nodal aggregation is visible in Fig. 4b-c. From this data, we note that particles aggregate at the nodal planes within seconds of switching on the SAW and are conveyed with the bulk velocity of the flow which for the experiment shown was 218 $\pm$ 6 μm s^{-1}. The nodal spacing, in this case 23 $\pm$ 3 μm, occurs as a result of the excitation of a half-wavelength resonance ($f = nc/2L$, where n = 10, c = 1600 m s^{-1}, and L = 250 μm) at the applied SAW frequency (λ = 50 μm) corresponding to the transverse dimension of the channel, L. This aggregation at the inlet junction nearest to the impinging SAW is shown in Fig. 4d. We note that the migration of the particles to a nearby node completes in just 4 s. It is also worth noting that different numbers of nodal planes are observed depending on the transverse dimensions of the channel.[21,32] This nodal aggregation could, in principle, be eliminated by augmenting the profile of the sidewalls to prevent coherent reflections from forming within the fluid bulk.[32]

Within the SAW aperture, acoustic streaming effects give rise to ostensibly chaotic dynamics[5] consisting of a complex collection of circulating cells with a variety of length scales, see Fig. 4e-f. This behavior is interesting and slightly counter-intuitive with respect to the steady unidirectional bulk flow found outside of the SAW aperture. In rectifying these two observations, we can speculate that either the tracer particles are being convected out of the bulk flow toward the base of these vortices where they become entrained at or near the substrate surface, or alternatively, particles reside in the fluid bulk but the net flow is simply not readily apparent owing to the complexity of the flow patterns. In either case, it is worth noting that within this SAW zone a large fraction of the particles that enter do in fact become entrained in this superposition of acoustic streaming induced vortices and standing waves. This aggregation, which is particularly strong near the SAW incident boundary, may have practical applications in bead based assays, for example, where particles must be retained throughout the introduction of a series of reagent changes and washes.

A similar closed-loop SAW pump arrangement was recently reported by Schmid *et al.*,[26] in which the impinging SAW is delivered to the working fluid *via* a liquid coupled glass superstrate[33] possessing a bonded PDMS microchannel. Like the approach presented here, this device more or less sidesteps the issue of SAW damping within PDMS, in this case by delivering the acoustic radiation through the floor of the microchannel—the SAW is projected at the Rayleigh angle through the fluid couplant and superstrate materials before encountering the working fluid—rather then tunneling directly through a bonded elastomeric interface. The fluid-coupled superstrate approach, despite being elegant, and attractive in terms of its modularity, is inherently limited. SAW energy must pass through a number of reflection sources each of which introduce loss. Additionally, the bulk irradiation of the fluid couplant and superstrate dissipate the incident SAW energy. Also inherent to this arrangement are numerous potential sources of error such as variation in couplant film thickness, unwanted evaporation, bulk streaming and convection, and misalignment.

In the Schmid device, for an applied input power of 29 dBm (794 mW) we estimate the pressure (using relevant channel dimensions and measured particle velocity) to be 7.94 Pa or 10.5 Pa/W. This result compares very well with their more rigorous obtained value of 4.8 Pa. Application of the same method for the device shown in Fig. 4 at an input power of 26 dBm (400 mW) produces a pressure of approximately 46 Pa or 116 Pa/W—a better than 10X increase in the conversion of acoustic energy to pressure driven flow.

In summary, we have introduced a simple and effective method for bonding standard machinable materials such as glass and silicon to piezoelectric substrates for the purpose of acoustofluidic integration. This methodology is performed at room temperature, mitigating the issues associated with traditional electrothermal bonding with these materials, while also eliminating the dependence on lossy elastomers. Devices prepared *via* this method display increased SAW transmission by as much as +20 dB (two orders of magnitude) compared to identical devices using the PDMS polymer, a dramatic improvement that will among other things reduce mechanical fatigue and greatly facilitate operation of such systems using battery operated modules. Furthermore, this bonding methodology enables tailorable selection of the bond thickness that in addition to enabling interesting new fabrication possibilities (*e.g.* adjustable spacers for planar flow vias), allows for the formation of sub-micron bond thicknesses by application of a modest compression force. Transmission of SAWs through these bonded interfaces was shown to depend upon both the base frequency as well as thickness of the bond relative to the SAW wavelength. It remains to be considered what the effects of the superstrate's material and geometric properties have on the overall performance of such devices, beside the possible specialised design of the IDTs to optimize the devices' overall performance. Doing so would likely result in even better performance in microfluidics applications. Apart from the native f^2 damping, optimal

Published on 10 May 2012 on http://pubs.rsc.org | doi:10.1039/C2LC40085E
Downloaded by Monash University on 19 July 2012

transmission was found to occur where bond interfaces could be classified as acoustically thin ($\delta \ll \lambda$) that, we anticipate, will guide the design of future closed-channel SAW microfluidic devices.

Acknowledgements

This work was performed in part at the Melbourne Centre for Nanofabrication, an initiative partly funded by the Commonwealth of Australia and the Victorian Government; JRF appreciates an MCN Technology Fellowship from this organisation and the Vice-Chancellor's Senior Research Fellowship from RMIT University. We gratefully recognize the following funding sources: Australian Research Council Discovery Grants DP0985253, DP1092955, and DP120100013 and the CSIRO Flagship Project Grant on Novel Sensors for Water Quality. LYY is grateful for an Australian Research Fellowship from the Australian Research Council.

References

1 L. Y. Yeo and J. R. Friend, *Biomicrofluidics*, 2009, **3**, 012002.
2 J. Friend and L. Y. Yeo, *Rev. Mod. Phys.*, 2011, **83**(2), 647–704.
3 Z. Wang and J. Zhe, *Lab Chip*, 2011, **11**, 1280.
4 Q. Zeng, F. Guo, L. Yao, H. W. Zhu, L. Zheng, Z. X. Guo, W. Liu, Y. Chen, S. S. Guo and X. Z. Zhao, *Sens. Actuators, B*, 2011, **160**(1), 1552–1556.
5 R. Shilton, J. Friend and L. Yeo, *Sens. Actuators, B*, 2011, **160**, 1565–1572.
6 A. Qi, P. Chan, J. Ho, A. Rajapaksa, J. Friend and L. Yeo, *ACS Nano*, 2011, **5**, 9583–9591.
7 A. Qi, J. R. Friend, L. Y. Yeo, D. A. V. Morton, M. P. McIntosh and L. Spiccia, *Lab Chip*, 2009, **9**, 2184.
8 M. K. Tan, L. Y. Yeo and J. R. Friend, *Appl. Phys. Lett.*, 2010, **97**, 234106.
9 R. Shilton, M. K. Tan, L. Y. Yeo and J. R. Friend, *J. Appl. Phys.*, 2008, **104**, 014910.
10 T. Franke, S. Braunmueller, L. Schmid, A. Wixforth and D. A. Weitz, *Lab Chip*, 2010, **10**, 789–794.
11 J. Shi, H. Huang, Z. Stratton, Y. Huang and T. Huang, *Lab Chip*, 2009, **9**, 3354–3359.
12 J. Shi, S. Yazdi, S. Lin, X. Ding, I. Chiang, K. Sharp and T. Huang, *Lab Chip*, 2011, **11**, 2319–2324.
13 M. Alvarez, J. R. Friend and L. Y. Yeo, *Langmuir*, 2008, **24**, 10629–10632.
14 Y. Bourquin, J. Reboud, R. Wilson and J. M. Cooper, *Lab Chip*, 2010, **10**, 1898.
15 Y. Bourquin, J. Reboud, R. Wilson and Y. Zhang, *Lab Chip*, 2011, **11**, 2725–2730.
16 R. J. Shilton, N. R. Glass, P. Chan, L. Y. Yeo and J. R. Friend, *Appl. Phys. Lett.*, 2011, **98**, 254103.
17 C. Eckart, *Phys. Rev.*, 1948, **73**, 68–76.
18 T. Squires and S. Quake, *Rev. Mod. Phys.*, 2005, **77**, 977–1026.
19 P. Rabiei and P. Gunter, *Appl. Phys. Lett.*, 2004, **85**, 4603.
20 M. Howlader, T. Suga and M. Kim, *Appl. Phys. Lett.*, 2006, **89**, 031914.
21 M. K. Tan, L. Y. Yeo and J. R. Friend, *Europhys. Lett.*, 2009, **87**, 47003.
22 S. Girardo, M. Cecchini, F. Beltram, R. Cingolani and D. Pisignano, *Lab Chip*, 2008, **8**, 1557.
23 Z. Guttenberg, H. Mller, H. Haberm ller, A. Geisbauer, J. r. Pipper, J. Felbel, M. Kielpinski, J. r. Scriba and A. Wixforth, *Lab Chip*, 2005, **5**, 308.
24 H. Takagi, R. Maeda and T. Suga, *J. Micromech. Microeng.*, 2001, **11**, 348.
25 D. C. Duffy, J. C. McDonald, O. J. A. Schueller and G. M. Whitesides, *Anal. Chem.*, 1998, **70**, 4974–4984.
26 L. Schmid, A. Wixforth and D. Weitz, *Microfluidics and Nanofluidics*, 201110.1007/s10404-011-0867-5.
27 L. Masini, M. Cecchini, S. Girardo, R. Cingolani, D. Pisignano and F. Beltram, *Lab Chip*, 2010, **10**, 1997–2000.
28 S. Martin and G. Frye, *Anal. Chem.*, 1994, **66**, 2201–2219.
29 C. Campbell, *Surface acoustic wave devices for mobile and wireless communications*, Academic Press, New York, 1998.
30 J. Friend and L. Yeo, *Biomicrofluidics*, 2009, **4**, 026502.
31 R. Arayanarakool, S. Le Gac and A. van den Berg, *Lab Chip*, 2010, **10**, 2115.
32 M. K. Tan, R. Tjeung, H. Ervin, L. Y. Yeo and J. Friend, *Appl. Phys. Lett.*, 2009, **95**, 134101.
33 R. Hodgson, M. Tan, L. Yeo and J. Friend, *Appl. Phys. Lett.*, 2009, **94**, 024102.

This journal is © The Royal Society of Chemistry 2012